Elastic–plastic analysis of the peel test for ductile thin film presenting a saturation of the yield stress

E. Simlissi, M. Martiny, Sébastien Mercier, S. Bahi, L. Bodin

Elastic-plastic analysis of the peel test for ductile thin film presenting a saturation of the yield stress.

E. Simlissi[a,b] and M. Martiny[a,*]and S. Mercier[a] and S. Bahi[a] and L. Bodin[b]

[a] Université de Lorraine, CNRS, Arts et Métiers ParisTech, LEM3, F-57000 Metz, France

[b] Cimulec, rue charles Picard, 57365 Ennery, France

Abstract

The paper investigates the peeling test of an elastic plastic film on an elastic substrate. The case of the film material presenting a saturation of the flow stress is considered. Based on earlier approaches of the literature, see for instance Kim and Aravas (1988) (Kim, K.S., Aravas, N., 1988, International Journal of Solids and Structures, **24**, 417-435), a semi-analytical expression for the plastic dissipation during bending/reverse bending is proposed. The validity of the present expression is established based on finite element calculations. It is shown that for the interpretation of results of peeling test at 90 degrees when the peeling force and the curvature have been measured, the present approach provides a precise interface fracture energy. The comparison is made with predictions based on an elastic perfectly plastic approach.

*Corresponding author, e-mail: marion.martiny@univ-lorraine.fr

Keywords : peel test, plastic dissipation, decohesion, Voce flow law, interface fracture energy

This is a pre-print of an article published in International Journal of Fracture. The final authenticated version is available online at: https://doi.org/10.1007/s10704-019-00393-7.

1 Introduction

Peeling is an affordable test conducted to determine the strength of the interface between two materials or between two layers. Depending on the mechanical behavior of the materials which form the interface, the prediction of the interface fracture energy from the measurement is not always straightforward. A large effort has been provided in the literature to analyse in details such experiments. For inextensible tape on a rigid substrate, Rivlin (1944) has observed that the peel force during steady state provides a direct measure of the interface fracture energy. From an energy balance, Kendall (1973) and Kendall (1975) have extended the Rivlin's approach to account for elastic contribution of the peel arm. Still in that configuration, the sole knowledge of the peel force provides an estimate of the interface fracture energy. The possibility to obtain this interface property when complex material behaviors are present needs the evaluation of the plastic dissipation during peeling. An important contribution has been proposed by Kim and Aravas (1988). From the moment curvature relationship for the peel arm (assuming pure bending under plane strain), the plastic dissipation is obtained. They investigate the case of materials presenting hardening (power law expression for the flow stress). Based on their work, the knowledge of the peel force and the slope of the film at the tip of the process zone is needed to predict the interface fracture energy. Kim et al. (1989) and Aravas et al. (1989) consider next an elastic perfectly plastic material. With

that specific behavior, an explicit moment curvature relation during the bending and the reverse bending is obtained. A closed form expression for the plastic dissipation is in addition proposed. As a consequence, from the energy balance of the peel test, the interface fracture energy can be derived from the knowledge of two experimental observations : force and angle at the tip. This model is efficient, has been adopted and discussed widely in the literature. Kinloch et al. (1994) analyse the case where the film may develop also plasticity during the test. Instead of considering a powerlaw relation for the hardening behavior as in Kim and Aravas (1988), they consider that for a certain class of material, the non linear response of the material can be modelled by a bilinear relationship. Therefore, an explicit expression for the plastic dissipation is also found. The model is shown to be salient for polyethylene film. Note that the configuration with a film material with a bilinear elastic plastic behavior was revisited by Moidu et al. (1998) mostly for the dissipation during reverse plastic unloading stage. One may also cite Williams and Kauzlarich (2005) for considering pre-strain and also non linear response. More recently, a large strain formalism has been proposed by Molinari and Ravichandran (2008) since during the decohesion process, the thin film may experience intense bending- reverse bending generating large strain. Close to the crack tip, the assumption of pure bending response may be questionable. Therefore, Wei and Hutchinson (1998) adopt finite element calculations to analyse in details the mechanical response of the system in the vicinity of the process zone, the detached arm still being analyzed with the bending approach. The interface response is modelled by introducing cohesive element. They also propose a clear parametric analysis of the peel test based on non dimensional parameters, see also Kim and Kim (1988). They clearly show that the interface fracture energy is depending upon the material parameters (elastic and plastic responses) and also properties of the cohesive el-

ement. Wei (2004) compares the bending model of Kim and Aravas (1988) and Aravas et al. (1989) with the combined model of Wei and Hutchinson (1998). Wei (2004) extends also the previous approach by accounting for the elastic compressibiliy. By still adopting a power law relationship for the hardening response of the film, a semi analytical expression is found for the link between moment and curvature during the bending, but it is not possible to provide a simple expression for the reverse bending phase. So clearly, as the material description becomes more complex, the possibility to derive analytical or semi analytical expression for the plastic dissipitation is reduced.

Wei and Zhao (2008) propose a critical assessment of the different methods (bending versus combined bending + FE approaches). They illustrate their findings on specific configurations for metallic films made of aluminium or copper on a ceramic. Peel tests are conducted at various angles (135 and 180) in addition to 90 degrees. The thickness of the Al film is varying from 20 to 200 microns. They also consider ultra thin film of copper deposited on the ceramic (from 1 to 15 microns). Based on the previous works (Wei and Hutchinson (1998), Wei (2004)), they conclude that the combined model (cohesive element and bending of the free arm) is valid for a weak interface strength. For a strong interface case, a full finite element model is preferable. Zhao and Wei (2007) confirm that a two parameters model is needed to obtain the interface fracture energy from a peel test. Instead of measuring the base angle at the crack tip, they measure the curvature of the film during the bending / reverse bending process. With these two informations (force + curvature), the strength of the interface can be determined precisely. They are also able to propose values for the cohesive law parameters (interface fracture energy and the separation strength). Experimental evidence based on copper thin fims is discussed. To analyse T-peel test on Cu/Cr/ polyimide system, Song and Yu (2002) determine the mechanical

response in tension of both Cu/Cr and polyimide. The plastic response of Cu is shown to saturate at very small plastic strain so the authors consider that copper has an elastic perfectly plastic response. From the theoretical expression of the plastic dissipation proposed by Kinloch et al. (1994), Kim and Aravas (1988) and Aravas et al. (1989), the interface fracture energy is obtained.

From Wei and Hutchinson (1998) and Zhao and Wei (2007), when the material response is known, the most important parameters controlling the decohesion are the interface fracture energy and the strength of the interface. They highlight that when the peel force and the curvature are measured in experiments, the interface fracture energy is theoretically found. The goal of the paper is to propose a contribution to the precise definition of the dissipated energy due to plasticity during bending - reverse bending for a particular class of material responses. Indeed, as shown in Song and Yu (2002), the flow stress of copper saturates rapidly. As a consequence, instead of adopting a perfectly plastic response as proposed in Song and Yu (2002), we propose to adopt a Voce type law to mimic such saturation like behavior. The paper is organized as follows. First the geometrical configuration and the material response are presented. In a second part, a semi analytical expression for the bending -reverse bending of metallic material with a Voce law is proposed. Therefore, the plastic dissipation can be derived. Closed form expression is provided in some specific cases. Finally, the proposed expressions are compared to the Aravas et al. (1989) approach and validated based on finite element simulations of peeling.

2 Configuration

A two layer woven composite / Cu sample is considered in this theoretical work. This configuration is representative of the one often present in printed circuit board. More generally, a system with a thick elastic substrate and a

thin ductile film can also be investigated through the proposed approach. As shown in Fig. 1 a), the metallic film thickness t is usually small compared to the one of the substrate (t between $17.5\mu m$ and $70\mu m$). Song and Yu (2002) have characterized electroplated Cu layer under uniaxial tension. The work hardening is very large at early deformation stage and presents a saturation like behavior for large plastic strain. Based on this observation, they analysed T-peel test by adopting the perfectly plastic analysis proposed by Aravas et al. (1989) and Kinloch et al. (1994). Instead of considering the material as an elastic perfectly plastic one, we propose to model its plastic response by adopting a Voce flow stress, Voce (1948). In that case, the mechanical response is written as :

$$\bar{\sigma} = E\bar{\epsilon} \quad \text{for} \quad \bar{\sigma} \leq \sigma_o \tag{1}$$

$$\bar{\sigma} = \sigma_o + Q(1 - \exp(-\gamma(\bar{\epsilon} - \epsilon_o))) \quad \text{for} \quad \bar{\sigma} > \sigma_o \tag{2}$$

where E is the Young modulus, $\bar{\sigma}$ the equivalent von Mises stress, $\bar{\epsilon}$ the accumulated strain and $\epsilon_o = \frac{\sigma_o}{E}$. The material is assumed incompressible. In the following of the paper, when plastic yielding is triggered, the flow stress (2) is written in a different way :

$$\bar{\sigma} = \alpha - \beta \exp(-\gamma\bar{\epsilon}) \tag{3}$$

with $\alpha = \sigma_o + Q$ and $\beta = Q \exp(\gamma\epsilon_o)$. With the present modelling, the initial yield stress is σ_o and the saturation value of the yield stress is α, see Section 3 and Fig. 2 for an illustration of the adopted response. The present work can be viewed as an application of the bending approach proposed by Kim and Aravas (1988) for a specific material response presenting a saturation of the flow stress.

The moment curvature relationship during peeling test is analysed assuming that 2D plane strain prevails, following the work of Kim and Aravas (1988),

Aravas et al. (1989), Kinloch et al. (1994) or more recently Wei (2004). The main equation of the analysis is recalled below with emphasis of the novelty in the moment curvature relationship due to the Voce law for plastic yielding. During the steady state phase of the test, any material point will experience a bending / reverse bending path, see Fig. 1 b). So the stress and strain tensors are (neglecting shear components) :

$$\boldsymbol{\sigma} = \begin{bmatrix} \sigma_{11} & 0 & 0 \\ 0 & \frac{\sigma_{11}}{2} & 0 \\ 0 & 0 & 0 \end{bmatrix} \quad \boldsymbol{\varepsilon} = \begin{bmatrix} \varepsilon_{11} & 0 & 0 \\ 0 & 0 & 0 \\ 0 & 0 & -\varepsilon_{11} \end{bmatrix} \tag{4}$$

In the elastic domain, path (OA), from the Hooke's law and owing to incompressibility, one has $\sigma_{11} = \frac{4E}{3}\epsilon_{11}$ while during plastic loading, $|\sigma_{11}| = \frac{2}{\sqrt{3}}\bar{\sigma}$. Pure bending is supposed to prevail so as in Kim and Aravas (1988), $\epsilon_{11} = -Kz$ where K is the curvature of the middle surface referred to the coordinate $z = 0$ and z is varying in the range $[-\frac{t}{2}, \frac{t}{2}]$. In Section 3, it will be shown that for a certain range of material parameters, even if the pure bending approach is not fully justified, the plastic dissipation during the peeling process is still accuratly estimated. This aspect was already mentioned in Kim and Kim (1988).

The bending moment per unit width of the metallic film is classicaly given by :

$$M = -\int_{-\frac{t}{2}}^{\frac{t}{2}} \sigma_{11} z dz = -2\int_{0}^{\frac{t}{2}} \sigma_{11} z dz \tag{5}$$

In the elastic phase of peeling (Path OA in Fig. 1 b), the moment curvature relationship is :

$$M = \frac{EKt^3}{9} \qquad 0 \leq K \leq K_e \tag{6}$$

with $K_e = \frac{\sqrt{3}\sigma_o}{Et}$.

For a ductile thin metallic film, the maximum curvature in point B of Fig.

1 b), K_B, is larger than K_e so plasticity plays an important role and a precise calculation of the dissipation is needed to extract from the measurement of the peel force, the true (or objective as named in Kim and Kim (1988)) interface fracture energy Γ. The moment curvature relationship during plastic loading (path AB) is :

$$M = -2\int_0^h \sigma_{11} z dz - 2\int_h^{\frac{t}{2}} \sigma_{11} z dz \tag{7}$$

where $h = \frac{\sigma_o\sqrt{3}}{2EK}$ corresponds to the position of the elastic-plastic transition when the curvature K is between K_e and K_B. Note that during the plastic loading and due to 2D plane strain, the accumulated strain is $\bar{\epsilon} = \frac{2}{\sqrt{3}} Kz$. Owing to the behavior (2) of the film, the expression (7) of the moment becomes :

$$M = \frac{8EKh^3}{9} + \frac{4}{\sqrt{3}}\int_h^{\frac{t}{2}} \left(\alpha - \beta \exp(-\frac{2\gamma K z}{\sqrt{3}})\right) z dz \tag{8}$$

By integration by parts, the integral term on the right hand side of Eq. (8) can be evaluated since :

$$\int_{z_1}^{z_2} z \exp(\delta z) dz = F(\delta, z_2) - F(\delta, z_1) \tag{9}$$

with the function F defined as $F(\delta, z) = \exp(\delta z)(\frac{z}{\delta} - \frac{1}{\delta^2})$. As a consequence, an explicit expression for Eq. (8) is found :

$$M = \frac{\alpha t^2}{2\sqrt{3}} + \frac{\sigma_o^2}{E^2K^2}(\frac{\sigma_o}{\sqrt{3}} - \frac{\sqrt{3}\alpha}{2}) - \frac{4\beta}{\sqrt{3}}\left[F(-\frac{2\gamma K}{\sqrt{3}}, \frac{t}{2}) - F(-\frac{2\gamma K}{\sqrt{3}}, h)\right] \tag{10}$$

From Eq. (2) when the material is perfectly plastic with $Q = 0$ (*i.e.* $\alpha = \sigma_o$ and $\beta = 0$), the relationship provided by Aravas et al. (1989) and Kim and Kim (1988) is recovered.

During the unloading phase, corresponding to path (BC) on Fig. 1 b), $(K_B - K_B^* \leq K \leq K_B)$, the moment is linked to the curvature, as in Kim and

Kim (1988) :

$$M = M_B + \frac{E}{9}(K - K_B)t^3 \tag{11}$$

where $M_B = M(K = K_B)$ given in Eq. (10). In the following, we denote $h_B = \frac{\sigma_o\sqrt{3}}{2EK_B}$ the position of the elastic plastic transition surface when the curvature is maximum, equal to K_B . The unloading phase stops in C when reverse plasticity develops at the outer surface of the film $z = \frac{t}{2}$. Let us denote $K_C = K_B - K_B^* \leq K_B$ the curvature leading to this condition. Following Kim and Aravas (1988) or Kinloch et al. (1994), the curvature K_C is defined as follows :

$$\frac{2\bar{\sigma}}{\sqrt{3}} = -\frac{2\bar{\sigma}}{\sqrt{3}} + \frac{4E}{3}(K_B - K_C)\frac{t}{2} \tag{12}$$

where $\bar{\sigma}$ stands for the yield stress prevailing at $z = \frac{t}{2}$ at the end of plastic bending phase (for $K = K_B$) : $\bar{\sigma} = \alpha - \beta\exp(-\frac{\gamma K_B t}{\sqrt{3}})$. As a consequence, $K_c = K_B - K_B^*$ with $K_B^* = \frac{2\sqrt{3}}{Et}(\alpha - \beta\exp(-\frac{\gamma K_B t}{\sqrt{3}}))$

For the peeling test, the reverse plastic loading, path (CD) on Fig. 1 b), exists, since the free arm is pulled into straight plane with a final curvature of $K_D = 0$. Let us denote $h^{'}(K)$ the position of the elastic-plastic transition during the reverse plastic loading. By construction, $h^{'}$ is larger than h_B, meaning that a material point with $z > h^{'}$ has already faced plasticity during the bending phase up to the curvature K_B. Similarly to Eq. (12), an implicit relationship for $h^{'}$ is found

$$\alpha - \beta\exp(-\frac{2\gamma K_B h^{'}}{\sqrt{3}}) = \frac{E}{\sqrt{3}}(K_B - K)h^{'} \tag{13}$$

In the theory as discussed by Aravas et al. (1989), the reverse plastic loading can continue for negative curvature. During peeling test, according to Fig. 1 b), such possibility is not considered here. For a given curvature $K_B - K_B^* \geq K \geq 0$, the film thickness is divided in three parts. For $0 \leq z \leq h_B$, the material is elastic. For $h_B \leq z \leq h^{'}$, the material is also in the elastic regime but has

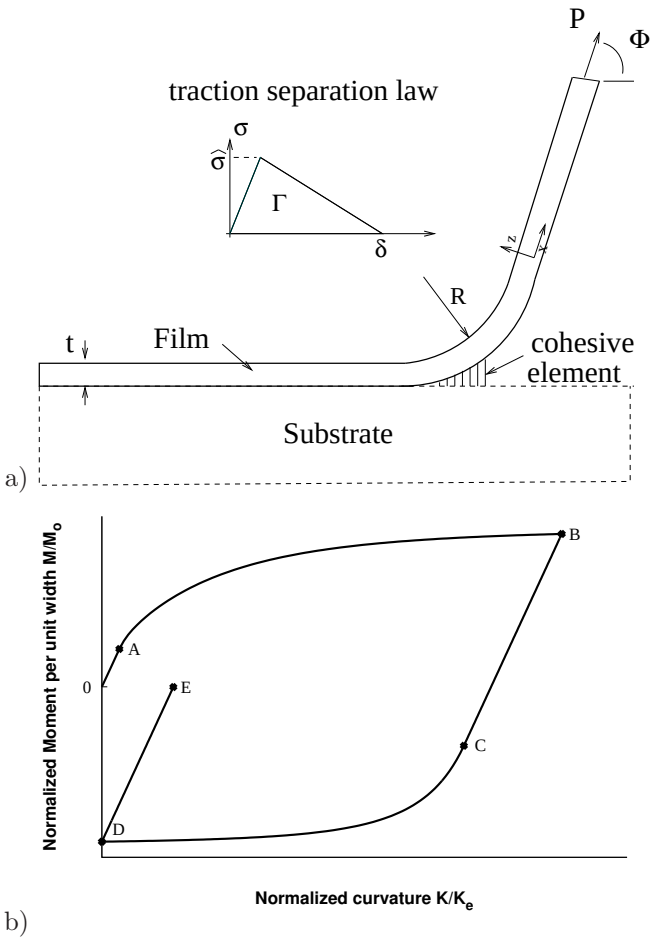

Figure 1: a) Peeling test configuration. The film thickness is t. The peel angle is Φ and the force per unit width is P. The traction separation law is also presented where $\hat{\sigma}$ represents the peak stress and Γ the interface fracture energy. A local coordinate system is adopted so that the position $z = 0$ corresponds to the middle plane of the film. During peeling, the film is bended. Let us note R the radius of curvature R of the top surface $z = \frac{t}{2}$. b) Schematic normalized moment versus normalized curvature under plane strain. Letters correspond to specific loading phase during the peeling test.

cumulated some plasticity during the bending stage (AB). Finally, in the third part $h^{'} \leq z \leq \frac{t}{2}$ the material point cumulates reverse plasticity. For the latter part of the film, the accumulated strain is, as given in Kim and Aravas (1988)

and Kinloch et al. (1994) :

$$\bar{\epsilon} = \frac{2}{\sqrt{3}} \left[(2K_B - K)z - \frac{\sqrt{3}}{E} \left(\alpha - \beta \exp(-\frac{2\gamma K_B z}{\sqrt{3}}) \right) \right] \tag{14}$$

By considering the three above strain histories, the moment can be evaluated in a semi analytical manner:

$$\begin{aligned} M = & \frac{8EK_B h_B^3}{9} - \frac{8E}{9}(K_B - K)(h^{'})^3 + \frac{2\alpha}{\sqrt{3}}(2(h^{'})^2 - h_B^2 - \frac{t^2}{4}) \\ & - \frac{4\beta}{\sqrt{3}} \left[F(-\frac{2\gamma K_B}{\sqrt{3}}, h^{'}) - F(-\frac{2\gamma K_B}{\sqrt{3}}, h_B) \right] + \frac{4\beta}{\sqrt{3}} \int_{h'}^{\frac{t}{2}} z \exp(-\gamma\bar{\epsilon}) dz \end{aligned} \tag{15}$$

with $h^{'}$ defined in Eq. (13) and $\bar{\epsilon}$ in Eq. (14). Note that when the curvature K_B and the parameter γ are large and the ratio $\frac{\sigma_o + Q}{E}$ is small (situation which is observed in peeling of copper film on an elastic substrate), the accumulated strain can be approximated by :

$$\bar{\epsilon} = \frac{2}{\sqrt{3}}(2K_B - K)z \tag{16}$$

In that case, a closed form expression for M defined in Eq. (15) is available. Indeed the integral term of the right hand side of Eq. (15) becomes :

$$\int_{h'}^{\frac{t}{2}} z \exp(-\gamma\bar{\epsilon}) dz = F(-\frac{2\gamma(2K_B - K)}{\sqrt{3}}, \frac{t}{2}) - F(-\frac{2\gamma(2K_B - K)}{\sqrt{3}}, h^{'}) \tag{17}$$

The domain of validity of this approximate solution will be discussed in Section 3.

As proposed by Kendall (1973), Aravas et al. (1989) or Wei and Hutchinson (1998) among others of the literature, the energy balance provides a link between the peeling force per unit width P (see Fig. 1 a), the interface fracture energy

Γ and the plastic dissipation Ψ :

$$P(1-\cos\Phi) = \Gamma + \Psi \quad \Rightarrow \quad \Gamma = P(1-\cos\Phi) - \Psi \tag{18}$$

Eq. (18) is valid assuming that the elastic stored energy of the system and other contributions are negligeable when compared to the contribution of plasticity during the bending, see for example Kim and Kim (1988) for further discussions. As mentioned by Kim and Aravas (1988), the plastic dissipation Ψ (or the work expenditure per unit film width) per unit crack advance is $\Psi = \int_L M dK$ where L is the loading path (OABCD) in the moment curvature Fig. 1 b) :

$$\Psi = \int_o^{K_e} M dK + \int_{K_e}^{K_B} M dK + \int_{K_B}^{K_B - K_B^*} M dK + \int_{K_B - K_B^*}^{0} M dK \tag{19}$$

Interestingly, the moment curvature relationship is known for the whole path (OABCD). Owing to the explicit expression on the path (OABC), the first three terms on the right hand side of Eq. (19) can be evaluated analytically. More details can be found in Appendix A. Finally, we obtained :

$$\begin{aligned}\Psi = \frac{\sigma_o^2 t}{6E} + \frac{\alpha t^2}{2\sqrt{3}}(K_B - K_e) + (\frac{\sigma_o}{\sqrt{3}} - \frac{\sqrt{3}\alpha}{2})\frac{\sigma_o^2}{E^2}(\frac{1}{K_e} - \frac{1}{K_B}) \\ - \frac{\sqrt{3}\beta}{\gamma^2}\left[G\left(-\frac{\gamma t}{\sqrt{3}}, K_B\right) - G\left(-\frac{\gamma t}{\sqrt{3}}, K_e\right)\right] + \frac{\sqrt{3}\beta}{\gamma}\exp(-\frac{\gamma\sigma_o}{E}) \\ (\frac{\sigma_o}{E} + \frac{1}{\gamma})(\frac{1}{K_B} - \frac{1}{K_e}) - M_B K_B^* + \frac{Et^3}{18}(K_B^*)^2 + \left[\frac{8EK_B h_B^3}{9}\right. \\ \left. - \frac{2\alpha}{\sqrt{3}}(h_B^2 + \frac{t^2}{4}) + \frac{4\beta}{\sqrt{3}}F(-\frac{2\gamma K_B}{\sqrt{3}}, h_B)\right](K_B^* - K_B) + I\end{aligned} \tag{20}$$

where the function $G(x,y)$ is defined as $G(x,y) = \frac{\exp(xy)}{y}$ and I given by :

$$\begin{aligned}I = \int_{K_B - K_B^*}^{0} \left[\frac{8E}{9}(K - K_B)(h')^3 + \frac{4\alpha}{\sqrt{3}}(h')^2\right. \\ \left. - \frac{4\beta}{\sqrt{3}}F(-\frac{2\gamma K_B}{\sqrt{3}}, h') + \frac{4\beta}{\sqrt{3}}\int_{h'}^{\frac{t}{2}} z\exp(-\gamma\bar{\epsilon})dz\right] dK\end{aligned} \tag{21}$$

The expression (20) is semi-analytical. Based on the present derivation, the plastic dissipation has almost a closed form expression except for the last term. Indeed, $h^{'}$, defined by the implicit relationship (13), is a function of the current curvature K. Nevertheless, when the radius of curvature is small (K_B large) and the parameter γ has an important value, then the accumulated strain (14) can be simplified, see Eq. (16). In addition, from Eq. (13), we propose to approximate $h^{'}$ by $h^{'} = \frac{\sqrt{3}\alpha}{E(K_B-K)}$. Based on these two assumptions, the last integral term I can be evaluated in closed form :

$$\begin{aligned} I^{approx} = \frac{4\alpha^3}{\sqrt{3}E^2}(\frac{1}{K_B} - \frac{1}{K_B^*}) - \frac{\sqrt{3}\beta}{\gamma^2}\Big(G(-\frac{\gamma t}{\sqrt{3}}, 2K_B) \\ -G(-\frac{\gamma t}{\sqrt{3}}, K_B + K_B^*)\Big) + \frac{\sqrt{3}\beta}{K_B\gamma^2}\Big(G(-2\frac{\gamma\alpha}{E}, \frac{K_B}{K_B^*}) \\ -G(-2\frac{\gamma\alpha}{E}, 1) + G(-2\frac{\gamma\alpha}{E}, \frac{K_B + K_B^*}{K_B^*}) - G(-2\frac{\gamma\alpha}{E}, 2)\Big) \end{aligned} \tag{22}$$

The present approach leading to the dissipation expression (20) contains by construction the perfectly plastic case. Indeed, when the parameter Q of Eq. (2) is set to zero, then obviously the material is elastic perfectly plastic. In that case, since $\alpha = \sigma_o$, one obtains $K_B^* = 2K_e$, $h_B = \frac{\sigma_o\sqrt{3}}{2EK_B}$. It is easily shown that the expression of Ψ is identical to the expression of the dissipation provided by Aravas et al. (1989) or Kim and Kim (1988) for a perfectly plastic case :

$$\Psi^{PP} = M_o K_e(2\frac{K_B}{K_e} - 5 + \frac{10}{3}\frac{K_e}{K_B}) \quad \text{when} \quad K_B \geq 2K_e \tag{23}$$

where $M_o = \frac{1}{2\sqrt{3}}\sigma_o t^2$ is the fully plastic moment.

Note also that when γ is becoming large, then the saturation occurs for low strain and therefore, it can be argued that the material is almost perfectly plastic with the yield stress being equal to the saturation stress $Q + \sigma_o$ (this assumption was adopted by Song and Yu (2002)). This case will be discussed in Section 3. One can also mention that the extension of the present approach

to a constitutive behavior containing a finite number of Voce law :

$$\bar{\sigma} = \sigma_o + \sum_{i=1}^{N} Q_i \left(1 - \exp(-\gamma_i(\bar{\epsilon} - \epsilon_o))\right) \tag{24}$$

is straigthforward. This can be done by imposing $\alpha = \sigma_o + \sum_{i=1}^{N} Q_i$, and replacing β by $\beta_i = Q_i \exp(\gamma_i \epsilon_o)$ and γ by γ_i. For sake of brevity, the corresponding expressions with the summation are not reproduced here.

3 Results

The first part of this section is devoted to the evaluation of the moment curvature response of a thin film under bending / reverse bending. The difference between the present development based on a Voce flow stress with the one of Kim and Kim (1988) for elastic perfectly plastic response is enlighted. In a second part, the interface fracture energy estimated based on the plastic dissipation during the bending /reverse bending is compared to the one imposed in the finite element simulation of the peeling test at angle $\Phi = 90$. Finally, the effect of the parameters of cohesive law on the peel force and curvature is investigated for peel tests at various angles Φ in the range $[45; 135]$.

3.1 Moment curvature response and plastic dissipation

The effect of the parameter γ of Eq. (2) on the elastic-plastic response of the metallic film is first investigated in Fig. 2. The reference parameters for the elastic plastic behavior of the film are listed in Table 1. The parameter γ influences the deformation level for which the flow stress approaches the plateau $\sigma_o + Q$. Indeed for a low value of γ (here $\gamma = 5$), a large strain is needed to reach the saturation regime (around $\bar{\epsilon} = 1$), while for a large value of γ (here $\gamma = 160$), a small strain is suffisant for the yield stress to reach the plateau

(around $\bar{\epsilon} = 0.03$). The initial plastic hardening modulus $\frac{\partial \bar{\sigma}}{\partial \bar{\epsilon}}(\bar{\epsilon} = \epsilon_o)$ is highly affected by the value of γ. For a metal, it must be lower than the elastic Young's modulus, leading to the condition for γ : $\gamma \leq \frac{E}{Q}$. With the present material parameters of Table 1, one obtains : $\gamma_{lim} = 361$.

Table 1: Reference parameters for the cohesive law and the elastic plastic behavior of the metallic film

t μm	E GPa	ν	σ_o MPa	Q MPa	γ	G_c N/m	$\hat{\sigma}$ MPa
35	65	0.26	100	180	5-160	1055	10

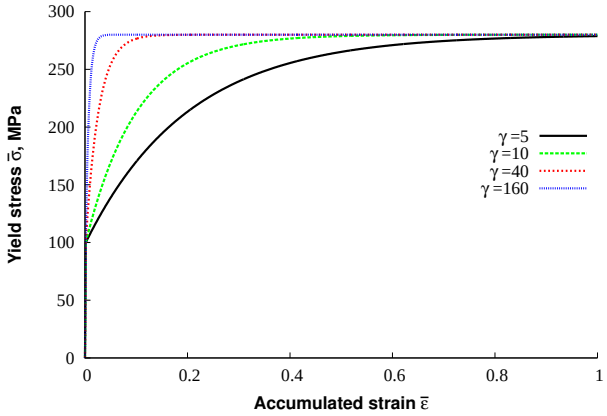

Figure 2: Elastic-plastic behavior of the metallic film. A Voce type behavior Eq. (2) is considered. Depending on the value of γ, the saturation state is approached for different accumulated strains.

It is also interesting to observe the difference between the moment curvature evolution predicted by adopting a Voce law and by assuming that the material is perfectly plastic. For illustration, in Fig. 3, a curvature for the metallic film of $K_B = 4000m^{-1}$ is adopted, leading to a radius of $0.25mm$. The film thickness is $t = 35\mu m$. Two perfectly plastic cases are considered. The first one assumes that the yield stress of the material is $\bar{\sigma} = \sigma_o$ while in the second case

$\bar{\sigma} = \sigma_o + Q$. As expected, the response based on the Voce law is located between the two curves corresponding to perfectly plastic materials. Since the plastic dissipation is the area formed by the curve along the path (OABCD), it is clear that assuming an elastic perfectly plastic behavior for the material is only valid for very large values of γ. It is interesting to notice that due to strain hardening, the moment curvature response during the reverse bending (path CD of Fig. 1 b) for $\gamma = 160$ corresponds closely to the response of a perfectly plastic material with $\bar{\sigma} = \sigma_o + Q$. Nevertheless, during the bending (path AB of Fig. 1 b), some difference exists which affects the total dissipation. On the contrary, for $\gamma = 40$, the plastic dissipation during the bending phase is strongly overestimated by assuming a perfectly plastic response. with $\bar{\sigma} = \sigma_o + Q$. Fig. 3 b) displays the evolution of the plastic dissipation Ψ as γ is enlarged, keeping $K_B = 4000m^{-1}$. It is observed that the plastic dissipation Ψ is increasing rapidly for small values of γ. As γ becomes larger, the response of the material becomes close to an elastic perfectly plastic response, see Fig. 2. As a consequence, the plastic dissipation saturates, reaching the value Ψ^{PP}, predicted by the elastic perfectly plastic approach of Aravas et al. (1989); Kim and Kim (1988). Theses trends are confirmed for two values of Q : $Q = 90$ or $180MPa$.

For material parameters of Table 1 and two values of γ : 40 and 160, the dissipation evaluated based on Eqs. (20) and (21) is presented in Fig. 4 a) for a curvature K in the range $1000m^{-1}$ to $10000m^{-1}$ leading to a radius of the film varying from $100\mu m$ to $1mm$. As expected, the plastic dissipation Ψ is larger when the normalized curvature is increased. For large value of the normalized curvature, the response is seen to be almost linear for both values of γ. This could have been anticipated. Indeed, Fig. 3 a) has shown that for large γ, the moment versus curvature response is quite similar to the one estimated based on a perfectly plastic approach. Therefore, in that case, the plastic dissipation

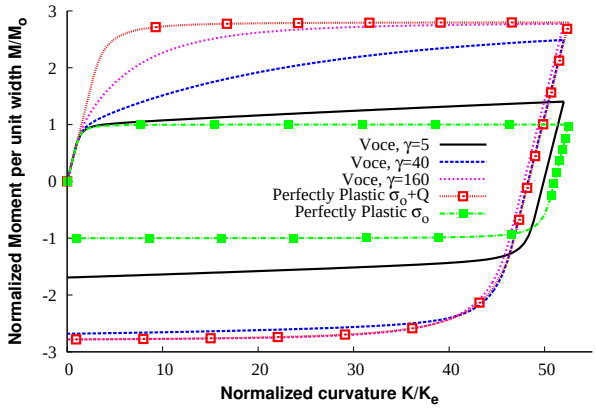

a)

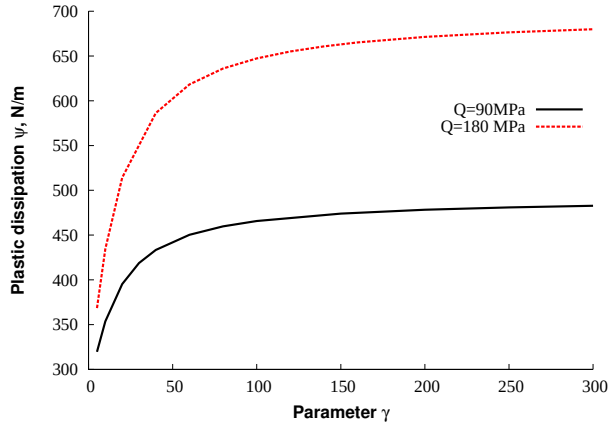

b)

Figure 3: a) Estimated moment curvature relationship for an elastic perfectly plastic material and a material with a Voce yield stress. Effect of the parameter γ controling the deformation for which the flow stress saturates, see Eq. (2). b) Plastic dissipation as a function of the parameter γ for two values of $Q = 90MPa$ and $Q = 180MPa$.

for a Voce or a perfectly plastic material (with $\bar{\sigma} = \sigma_o + Q$) must be quite similar. From Eq. (23), the increment of plastic dissipation $\Delta\Psi$ produced by an increment of the normalized curvature $\frac{\Delta K}{K_e}$ is expressed as follows, when $\frac{K}{K_e}$ is large :

$$\Delta\Psi = \frac{\sigma_o(\sigma_o + Q)t}{E}\frac{\Delta K}{K_e} \tag{25}$$

With the parameters of Table 1, we observed that $\Delta\Psi \approx 15\frac{\Delta K}{K_e}$. This is consistent with the observation of Fig. 4 a). In addition, for the two values $\gamma = 40$ and $\gamma = 160$, we have observed that the approximate dissipation based on Eq. (22) almost coincides with the one obtained with Eq. (20) (results not presented here).

Next, a more precise comparison between the predicted dissipation ψ evaluated based on the Voce law and based on a perfectly plastic response ψ^{PP} (with $\bar{\sigma} = \sigma_o + Q$) is presented in Fig. 4 b). For the value $\gamma = 40$, the normalized ratio $\frac{\psi}{\psi^{PP}}$ is still below 0.9 when the normalized curvature $\frac{K}{K_e}$ is equal to 88 ($K = 6676m^{-1}$ or a radius of $149\mu m$). Adopting a perfectly plastic aproximation for this material when analyzing results of peeling test will lead to a 10% difference in the interface fracture energy Γ, see the energy balance equation (18) for a test at $\Phi = 90^o$. When $\gamma = 160$, we clearly observed that for $\frac{K}{K_e} = 88$, less than 3% difference remains. Note that Fig. 3 was constructed with a value of the curvature of $K_B = 4000m^{-1}$ ($\frac{K_B}{K_e} = 52$). In that case, a difference of 15% exists between Ψ based on expression (20) and Ψ^{PP} for $\gamma = 40$ while for $\gamma = 160$, the difference reduces to 4%.

3.2 Finite element validation based on peeling test

In this section, we propose to analyze in more details the peeling test on a two layer woven composite /Cu sample. The plastic behavior of copper is described by Eq. (2). The substrate, representative of a woven composite used in printed circuit board industry remains elastic. The elastic behavior has been identified based on the strategy proposed in Girard et al. (2018). The in plane Young modulus is around 20.6 GPa, while the out of plane one is 16.4 GPa. The in plane Poisson ratio is 0.17.

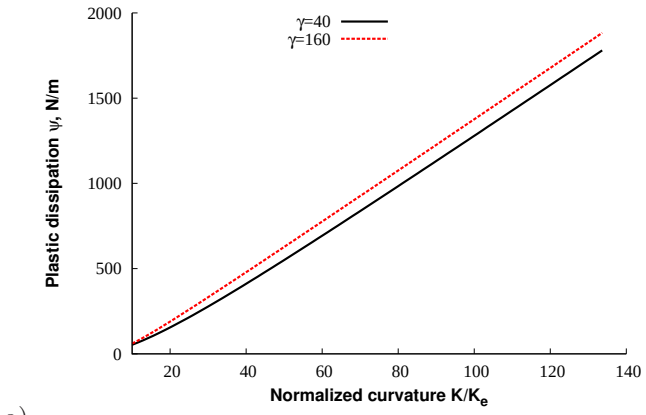

a)

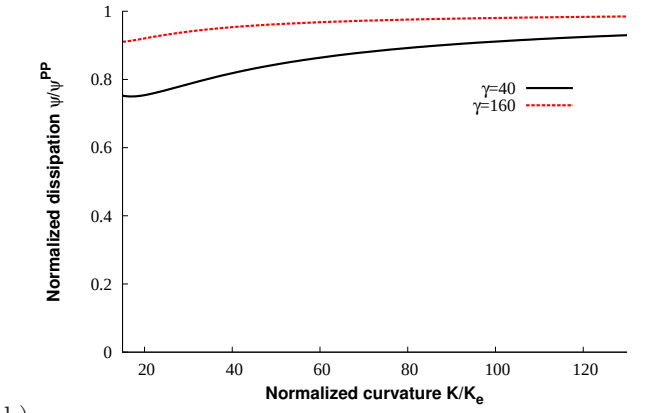

b)

Figure 4: a) Plastic dissipation versus normalized curvature K/K_e during bending and reverse bending for two values of γ : $\gamma = 40$ and $\gamma = 160$. b) Ratio between the plastic dissipation evaluated based on a Voce flow stress and a perfectly plastic response. Material parameters for the Voce law are given in Table 1.

A Finite Element model of peeling test under plane strain conditions for various angles Φ has been considered on ABAQUS Software, see Fig. 1 a). The interface is modeled with cohesive elements : a bilinear separation law in mixed mode is considered. For limited separation of the interface, the response is linear $\sigma_n = K_{nn}\delta_n$ and $\sigma_t = K_{tt}\delta_t$, with $K_{tt} = K_{nn} = 10^6 N/mm^3$ the initial stiffness of the cohesive element. σ_n, σ_t are the normal and tangential component of

the traction force. δ_n and δ_t are the corresponding separation displacement at the level of the cohesive element. The following quadratic failure initiation and linear failure criterions are adopted :

$$\left(\frac{\sigma_n}{\hat{\sigma}_{n,c}}\right)^2 + \left(\frac{\sigma_t}{\hat{\sigma}_{t,c}}\right)^2 = 1 \qquad \frac{G_n}{G_{n,c}} + \frac{G_t}{G_{t,c}} = 1 \tag{26}$$

with $G_n = \int \sigma_n d\delta_n$ and $G_t = \int \sigma_t d\delta_t$. Such cohesive law is implemented in the ABAQUS software, see ABAQUS (2013). More information can be found elsewhere. Note that other choices for the cohesive law could have been adopted. Discussion about mixed mode ratio can be found in Tvergaard and Hutchinson (1993), Kinloch et al. (1994), Wei (2004) and Martiny et al. (2008). In our FE simulations, as in the literature on that subject, only two parameters are kept for the definition of the cohesive law by imposing : $\hat{\sigma}_{n,c} = \hat{\sigma}_{t,c} = \hat{\sigma}$ and $G_{n,c} = G_{t,c} = G_c$. $\hat{\sigma}$ represents the peak stress and G_c the fracture energy, which corresponds here to the interface fracture energy Γ, see Fig. 1 a).

The goal of the finite simulations is to provide values of the peel force and the curvature for a given cohesive law and a given material behavior for the thin film. Knowing the curvature, the plastic dissipation can be evaluated by Eq. (20). Subsequently, the interface fracture energy Γ is derived from the energy balance (18). The predicted value for Γ is compared to the one adopted in the FE simulation. The reference parameters for the cohesive law and for the elastic plastic behavior of the film are listed in Table 1.

Plane strain elements (CPE4R) are adopted with 9 elements in the film thickness for $\Phi < 90$. For $\Phi \geq 90$, 18 elements in the film thickness are considered since the curvature is smaller (sometimes around $100\mu m$ for $\Phi = 135$). A mesh sensitivity study has been carried out by considering larger mesh density. By increasing the number of elements, and therefore by reducing the element size,

the predictions in terms of peel force and curvature are preserved. The cohesive element size in the 1 direction is five times lower than the element size in the film. The height of the cohesive element is vanishing small. In all calculations, the velocity for the peeled arm is $V = 0.5mm/s$. To ensure that the peel angle Φ remains constant during the FE simulation, the substrate is moving in the horizontal direction with the same velocity $V = 0.5mm/s$. Note that the length of the substrate is 50 mm long. It has been checked that a stationary process prevails after a quite short time period.

First we present a comparison of the model capability based on a peeling test with $\Phi = 90$. This working condition is the most often used in the literature and for practical applications. For instance, a peeling test at $\Phi = 90$ is recommended for the printed circuit board industry to evaluated the interface strength, see the IPC-TM-650 2.4.8 standard. The force versus time is presented in Fig. 5 for three values of the γ parameter : 5, 40 and 160 and for two values of Q : 90 and 180 MPa. A stationary process for the peeling force is established after $3s$. We clearly observed that for the same interface fracture energy $\Gamma = 1055N/m(orJ/m^2)$, the force is larger when γ increases. Indeed, for $Q = 180MPa$, the level of the force is evolving from $1531N/m$ with $\gamma = 5$ to $1707N/m$ for $\gamma = 160$. As Q is larger, meaning that the plateau value for the yield stress is larger, the peeling force is also enhanced significantly for large values of γ. Remember that as the parameter γ is large, the saturation stress is reached for lower strain, see Fig. 2. From the energy balance (18), and since Γ is fixed, this enhancement of the force means that the plastic dissipation is larger. A key factor controling the plastic dissipation is the maximum curvature K_B, existing at the end of the loading path (AB).

During the stationary process in the FE simulations, the radius of curvature R of the top surface $z = \frac{t}{2}$ can be measured, see Fig. 5 b) where a zoom is

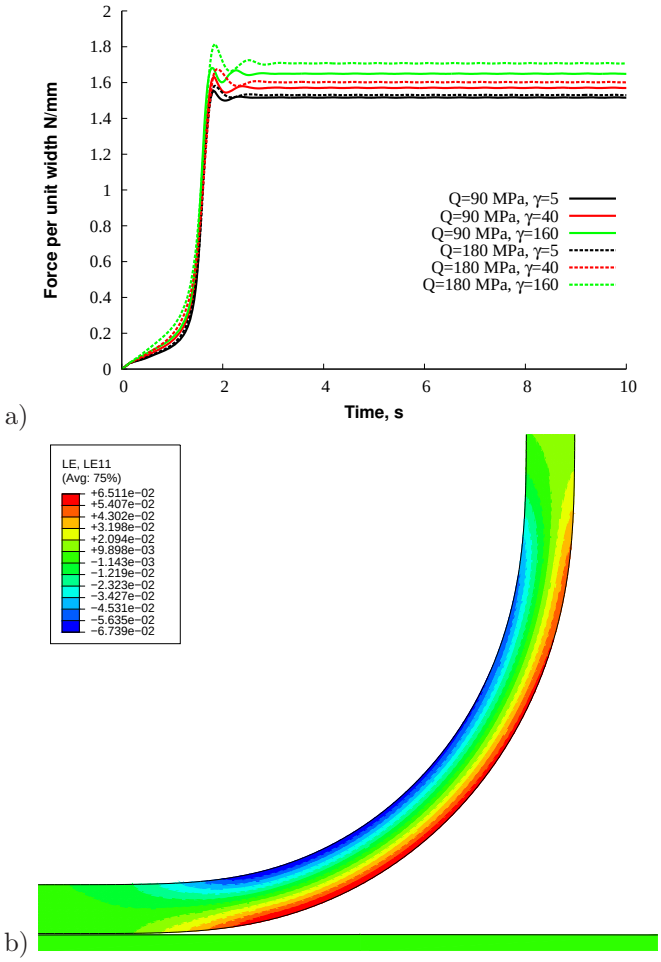

Figure 5: a) Force per unit width versus time. Different values of material parameters Q and γ are tested. b) View of the film curvature during the bending / reverse bending process. The cohesive elements are removed for presentation purpose. The longitudinal strain E_{11} is displayed. A local orientation is adopted so that the direction 1 is always parallel to the middle surface, as presented in Fig. 1.

presented in the area where the thin film is detached from the substrate. It is observed in this figure, that in the case of a peel test with an angle of $\Phi = 90^o$, the film is curved with a radius R, which is assumed to be representative of the curvature at point B of Fig. 1 b). To be consistent with the bending

model where the curvature is measured from the middle surface of the film, the curvature K_B is related to R by $K_B = (R + \frac{t}{2})^{-1}$. Fig. 6 presents the corresponding evolution of the curvature versus γ for the two different values of Q. The evolution of the curvature versus γ is not monotonic. For moderature values of γ, K_B is first decreasing. Then K_B reaches a minimum value and then subsequently increases slightly as γ becomes larger. Note also that depending on the respective value of Q which is scaling the saturation of the flow stress, the minimum of the curve is reached for larger γ value as Q is larger. The non monotonic trend can be understood as follows. On the one hand, from Fig. 5, it is seen that when γ is increasing from 5 to 40, the level of the force is slightly increased. From the balance of energy, the larger force level is linked to an increase in plastic dissipation. Nevertheless, in Fig. 3 b), it has been shown that, when γ is increasing from 5 to 40, the plastic dissipation is strongly enhanced, for a fixed curvature. As a consequence, to preserve the balance of energy and the slight increase of the force, the curvature is reduced so as to propose a moderate increase in plastic dissipation. On the other hand, when γ is large, the plastic dissipation saturates when assuming that the curvature remains constant, see Fig. 3 b). Therefore, the larger peeling force observed for γ=160 when compared to $\gamma = 40$ originates from the increase of the curvature, which produces larger dissipation.

The prediction of the plastic dissipation can be obtained via Eq. (20) based on the curvature K_B captured by the finite element calculation (Fig. 6). In addition, from the numerical measurement of the peeling force (Fig. 5), and from Eq. (18), the interface fracture energy is estimated. The result of the dialog between the present model and the finite element calculation is illustrated in Table 2 where are presented the predicted values for Γ adopting the dissipation

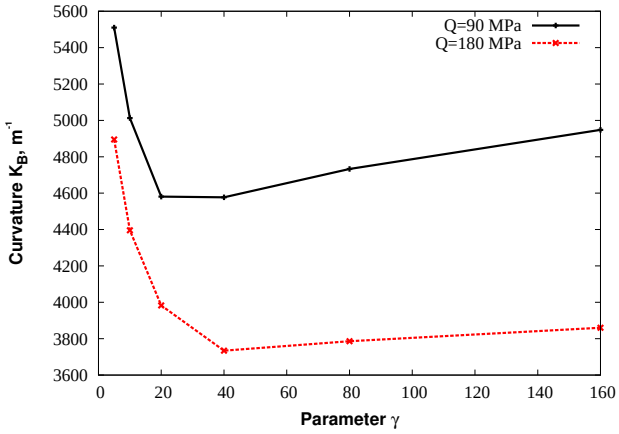

Figure 6: Effect of the γ parameter of Eq. (2) on the curvature K_B of the film during a peeling test at $\Phi = 90$. The ductile film behavior is elastic plastic with a flow stress described by a Voce equation (2). Material parameters are listed in Table 1.

estimate provided by the current approach Eq. (20), the approximate evaluation of the plastic dissipation based on Eq. (22) and the perfectly plastic dissipation Eq. (23). The obtained values are compared to $\Gamma = 1055N/m$, which is the prescribed value in the finite element simulations. All the results concern a peel test at an angle $\Phi = 90$. Our present approach is able to predict the Γ value with less than 1.5% in the whole range of γ for the two considered cases $Q = 90MPa$ and $Q = 180MPa$, see Table 2. As expected, adopting the formula (23) proposed by Aravas et al. (1989) is only valid when γ is larger than 40. In that case, the stress strain response in tension is quite similar to one expected when the material is elastic perfectly plastic, see Fig. 2. Note also that estimation of the interface fracture energy based on the approximate solution Eq. (22) is also accurate for the values of the γ parameter considered in the present paper. This observation confirms a previous finding where very limited difference was observed between predictions of the interface fracture energy based on Eqs (20) and (22) for results of Fig. 4.

Table 2: Predicted interface fracture energy. From the force and curvature measured owing to finite element simulations (here $\Gamma = 1055N/m$, $\Phi = 90$), the plastic dissipation is evaluated based on the present approach (20), on the approximate solution (22) and on the perfectly approach of Aravas et al. (1989), see Eq. (23). From the energy conservation (18), the interface fracture energy is estimated.

Estimated Γ (N/m) for $Q = 90MPa$

γ	5	10	20	40	80	160
Γ from Eq. (20)	1056	1053	1050	1054	1046	1044
Γ from Eq. (22)	1051	1050	1048	1053	1045	1043
Γ^{PP} (23)	831	891	946	995	1014	1028

Estimated Γ (N/m) for $Q = 180MPa$

γ	5	10	20	40	80	160
Γ from Eq. (20)	1052	1047	1050	1058	1069	1066
Γ from Eq. (22)	1031	1035	1044	1055	1060	1066
Γ^{PP} (23)	662	769	873	956	1007	1041

Fig. 7 a) presents the time evolution of the strain component E_{11} for three points located on the top of the film ($z = 16.6$, 14.6 and $12.6\mu m$) and 3 on the bottom of the film ($z = -16.6$, -14.6 and $-12.6\mu m$). As expected, the points located at the bottom (resp. top) of the film $z < 0$ (resp. $z > 0$) experience positive (resp. negative) value for the strain component E_{11}. The maximum strain is reached when the curvature is maximum, loading condition B of Fig. 1 b). During the unloading stage (BC), the strain is slightly decreasing while in the reverse bending phase (CD), the strain magnitude is strongly reduced. Nevertheless, due to plasticity development and presence of the peeling force, a residual strain still exists in the peel arm. The residual strain is homogeneous in the thickness, meaning that the curvature is close to $K_D = 0$ (straight arm at the end). It is also interesting to mention that for the condition presented here ($\Phi = 90$), the strain profile in the thickness is almost skew symmetric. This is in close agreement with the bending theory of the beam which is based on the assumption that any material point entering into the process zone will experience pure bending /reverse bending $E_{11} = -Kz$. Fig. 7 b) presents the

strain development inside the film thickness at the exact end of the bending process, condition B. Since K_B can be evaluated from the finite simulations, the theoretical predictions of the strain $E_{11} = -K_B z$ is also added to the FE strains. We observe that for a peel angle of $\Phi = 90$ where $K_B = 3759m^{-1}$ and $R = 248\mu m$, it exists a very good agreement between the theory and the FE results. A similar comparison is made for two other angles : $\Phi = 60$ and $\Phi = 135$. For $\Phi = 135$, it is seen that the strain distribution is non linear, with a larger absolute value of the strain at the bottom surface when compared to the top surface. In that configuration $K_B = 6468m^{-1}$ corresponding to a radius of $R = 137\mu m$. It will be shown next that the limited correlation of the present theory in reproducing the expected value of the interface fracture energy is partially due to the observed small radius. This conclusion was already drawn in Aravas et al. (1989). Indeed, the plane strain bending approach is considered by Hill (1950) as a good approximation assuming that the minimum radius is larger than four to five times the film thickness. With $t = 35\mu m$ and $\Phi = 135$, R is smaller than $4t$. For $\Phi = 60$, $K_B = 2434m^{-1}$ and $R = 393\mu m$, the strain response is affine. The main difference comes from the fact that the condition $E_{11} = 0$ is observed for $z = 5\mu m$ while in pure bending as in the proposed theory, this condition is fulfilled for $z = 0$. Clearly, for $\Phi < 90$, instead of pure bending, a more complex loading path prevail with bending and extension.

Fig. 8 presents the stress-strain loading path faced by 6 material points inside the thickness during the peeling process for two angles : $\Phi = 90$ and $\Phi = 135$. The loading stages (OABCD) are also added in Fig. 8 a). The material parameters are listed in Table 1 with $\gamma = 40$. In Fig. 8 a), for an angle $\Phi = 90$, we clearly observed that the assumption of pure bending / reserve bending is mostly satisfied. During the loading path (OAB), the trajectory of all points in the stress-strain plane is identical up to a maximum strain $E_{11}^{max} = -K_B z$.

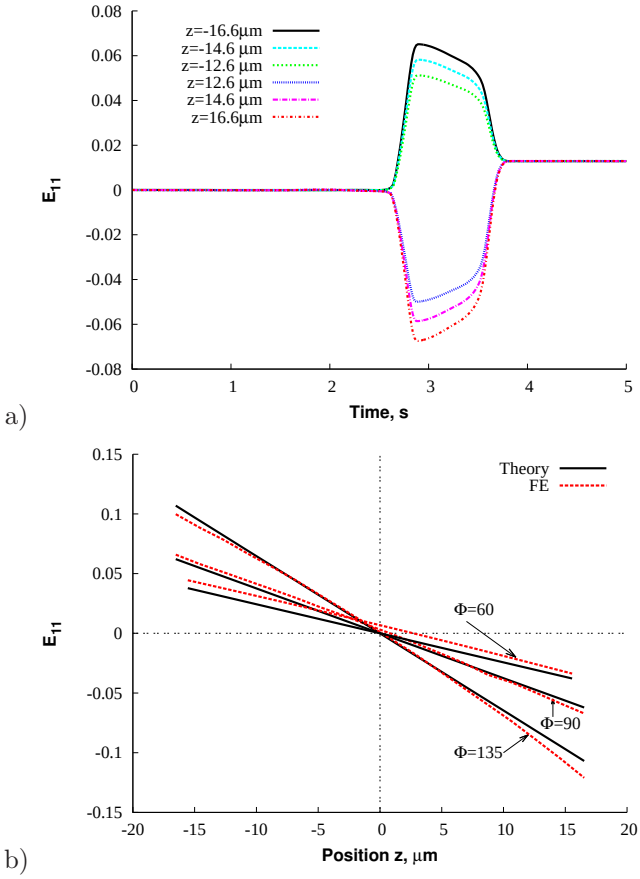

Figure 7: a) Time evolution of the longitudinal strain component E_{11} within the film thickness for the peel angle $\Phi = 90$. b) Maximum through thickness longitudinal strain captured by the Finite element. Comparison with the bending approach for three peel angles : 60^o, 90^o and 135^o. Material parameters are those of Table 1 with $\gamma = 40$.

It is observed that for the material points located close to the external surface of the film, the strain cumulated up to B is large enough so that the flow stress has already reached its saturation value $\sigma_o + Q$. Therefore during the reverse bending process (CD), the stress level remains almost constant. In that stage, the material behavior can be approximated by an elastic perfectly plastic response. For $\Phi = 135$ (see Fig. 8 b)), the same conclusion is made except for

the maximum strain. Indeed, we observed that the maximum longitudinal strain at the top surface is 20% larger in absolute value than the strain experienced at the bottom surface. From the knowledge of the curvature K_B, the theoretical prediction of the stress σ_{11} versus strain E_{11} response is also added to Figs 8 a) and b) for two points located at $z = \pm 16.6 \mu m$ (see dotted lines with squares or circles). It is clearly observed that some discrepancy is shown for the theory when compared to the finite element response. Of course, in the theory, a skew symmetric distribution of strain is assumed, which is not clearly the case in the Finite Element simulations. The bending assumption is better fulfilled for $\Phi = 90$ than for $\Phi = 135$.

At least for the parameters adopted as reference in Table 1, the proposed expression Eq. (20) for the plastic dissipation enables to recover precisely the interface fracture energy inserted in the numerical calculations when the peel angle is $\Phi = 90$, as presented in Table 2. Peeling tests with an angle in the range $[+45, +135]$ were also simulated by FE. The reference parameters of Table 1 are still adopted with $\gamma = 40$. Fig. 9 displays the estimated value of the fracture energy Γ assuming that the force per unit width P and the maximum curvature K_B are known quantities (obtained from FE simulations). As already mentioned, the pure bending theory predicts a consistent interface fracture energy using Eqs (18) and (20). It is observed that for $\Phi = 120, 135$, the estimate for Γ is $1160 N/m$, instead of $1055 N/m$. Clearly, the film radius is too small when compared to the film thickness for the bending theory to be accurate, see Hill (1950). For $\Phi = 45, 60$, the strain map in the film thickness is neither fully consistent with a pure bending approach, see Fig. 7 b). Indeed, for $\Phi < 90$, the stretching of the film is more intense, and the tensile contribution is noticeable. It is observed that while for $\Phi = 60$, the estimation of Γ is still accurate (less

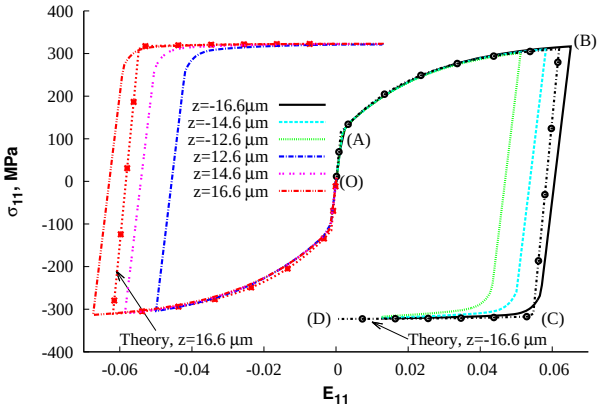

a)

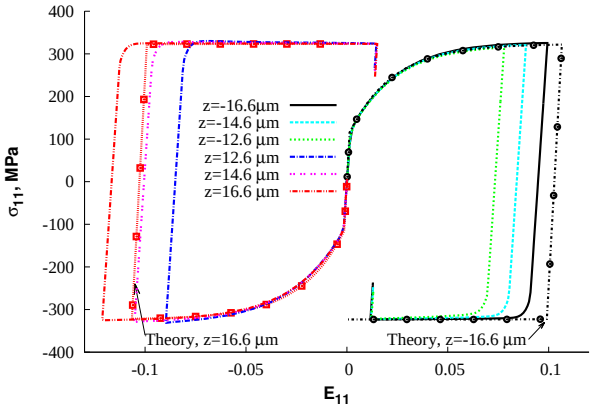

b)

Figure 8: Loading path faced by material points along the thickness during the peeling process. a) Peel angle of 90^o b) Peel angle of 135^0. A local orientation is adopted in the Finite element simulations. The reference parameters are those of Table 1 with $\gamma = 40$.

than 5% difference, $\Gamma(60) = 990N/m$), the situation is different for $\Phi = 45$ with more than 10% difference, $\Gamma(45) = 909N/m$. The prediction of Γ based on the approximate relation (22) is not presented since it coincides almost with the one given by Eq. (20). The prediction of Γ based on the perfectly plastic approach Eq. (23) is also superimposed to Fig. 9. The perfectly approach is underestimating Γ for the considered material parameters, except for the large angle

condition with $\Phi = 135$ or $\Phi = 120$. So from Fig. 9, it can be mentioned that the estimation of the interface fracture energy can be reasonably captured by the present work, from the knowledge of the experimental force and curvature for tests with peel angle around $\Phi = 90$. Interestingly, it is seen that the closed form expression derived from Eq. (22) provides also consistent estimate and can be used instead of Eq. (20).

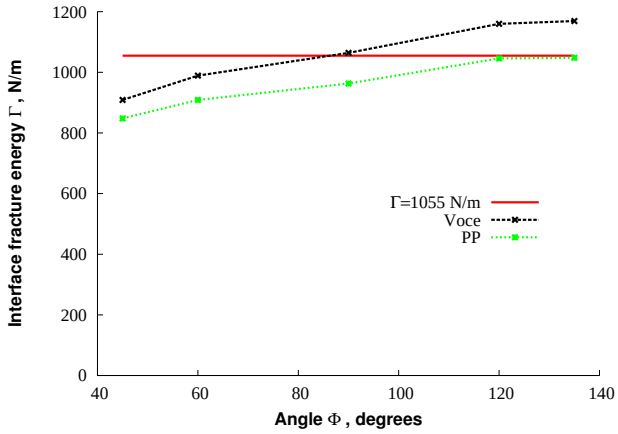

Figure 9: Effect of the angle on the estimated interface fracture energy. The predictions based on the present work Eq. (20) and on the equation (23) derived for perfectly plastic material are compared. The material parameters are listed in Table 1 with $\gamma = 40$.

From previous works of the literature (Wei and Hutchinson (1998) , Kim and Kim (1988), Wei (2004)), the results of finite element simulation of peeling tests in presence of plasticity are highly influenced by the properties of the interface, *i. e.* the parameters of the cohesive law (the interface fracture energy Γ and the peak stress $\hat{\sigma}$). Next, we propose to investigate their relative influence on the force and curvature during a peel test. The material behavior is still described by a Voce law with parameters listed in Table 1 and $\gamma = 40$. We assume that for a given angle $\Phi = 90$, the force P is known. For different values of Γ, the

peak stress $\hat{\sigma}$ is adjusted so that the force P at $\Phi = 90$ is reproduced, see Martiny et al. (2008). In Fig. 10, the evolution of the peeling force and the curvature K_B are displayed for 6 sets of parameters (Γ, $\hat{\sigma}$) defined in Table 3. Each of the set leads to the same force per unit width P for $\Phi = 90$. As Γ is reduced, the peak stress has larger value leading to a larger curvature (small radius R) so that the plastic dissipation is enlarged. For $\Gamma = 1055N/m$ and $\hat{\sigma} = 10MPa$, finite element simulation of the peel test at $\Phi = 90$ has provided a curvature of $K_B = 3759m^{-1}$ (a radius $R = 248\mu m$) while for $\Gamma = 527.5N/m$ and $\hat{\sigma} = 72MPa$, the curvature is $K_B = 6042m^{-1}$ corresponding to a radius of $R = 148\mu m$. After this calibration, the force P is evaluated for four other angles $\Phi = 45, 60, 120$ and 135. Fig. 10 shows that the force is quite insensitive to the set (Γ, $\hat{\sigma}$) for $\Phi > 90$. On the contrary, there is an important influence on the force prediction for angles lower than 90. This effect is larger for $\Phi = 45$ than for $\Phi = 60$. For instance, with $\Phi = 45$, one has $P = 3777N/m$ for $\Gamma = 1055N/m$ and only $P = 3300N/m$ when the interface fracture energy is reduced by a factor of two $\Gamma = 527.5N/m$. Remember that $\hat{\sigma}$ is adjusted so as to preserve the force level at $\Phi = 90$ degree. Fig. 10 enligthens also that the curvature is the most sensitive feature to any variation of the set (Γ, $\hat{\sigma}$). Therefore, to identify from peeling tests the interface fracture energy, one can act as follows. A peeling test carried out at $\Phi = 90$ where the force and curvature are recorded may be sufficient to provide a consistent value for Γ. Nevertheless, it seems important also to validate this estimate by confirming the predictions of the force for another test; a peeling test at angle $\Phi = 45$ seems to be a good candidate. Indeed, the force P for low angle Φ is sensitive to the interface fracture energy. In that case, a finite element simulation of the considered configuration must be carried out. Of course, all the present results are valid for the specific cohesive law (26) and for the given material behavior.

Table 3: Couples (Γ, $\hat{\sigma}$) leading to the same force per unit width for the peel angle $\Phi = 90$.

Γ [N/m]	1055	949.5	844	738.5	633	527.5
$\hat{\sigma}$ [MPa]	10	15	21	31	46	72

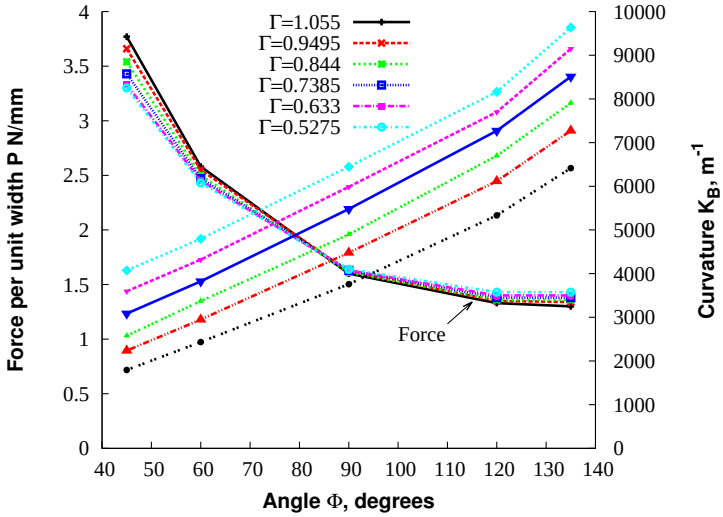

Figure 10: Force per unit width and curvature for various peeling angles Φ. Note that the cohesive law parameters listed in Table 3 are adjusted so that the peeling force $P(\Phi = 90)$ is preserved for all angles.

4 Conclusion

The estimation of the plastic dissipation during bending / reverse bending for a Voce type behavior is the main goal of the present work. A semi-analytical expression is provided for the plastic dissipation. As expected, the plastic dissipation is highly sensitive to the curvature. As proposed previously in the literature for other material constitutive laws, the knowledge of the dissipation enables to evaluate the interface fracture energy from the peeling force measurement. By comparison with finite element calculations performed for various angles in the range $[45, 135]$, it is found that the present theory is accurate to analyse peeling test for $\Phi = 90$ and provide a satisfactory estimate for other peel

angles. For $\Phi = 90$, at least for the material parameters adopted in the present paper, the assumption of pure bending in the process zone is a quite satisfactory hypothesis. It is also observed that depending on the material parameters, the perfectly plastic approach proposed by Kim and Kim (1988), Aravas et al. (1989) can also be justified even for a Voce type material when the saturation of the flow stress is observed for limited strain.

The cohesive law parameters (interface fracture energy and peak stress) can be estimated by an inverse method, assuming that the force and curvature have been identified with recourse to finite element simulations or experiments. The identification of the cohesive law parameters could benefit from a further validation based on peeling tests carried out mostly for low peel angle $\Phi < 90$.

Acknowledgements

The authors acknowledge the support of Agence Nationale de Recherche through the program Labcom LEMCI ANR-14-LAB7-0003-01.

The research leading to these results has received funding from the European Union's Horizon 2020 research and innovation programme (Excellent Science, Marie Sklodowska-Curie Actions) under REA grant agreement 675602 (OUTCOME project).

A Derivation of the expression for the plastic dissipation

The present appendix provides some details concerning the derivation for the expression of the plastic dissipation Ψ along the loading path (OABCD). For the elastic response of the film along path (OA), as depicted in Fig. 1 b), one

obtains from Eq. (6):

$$\int_0^{K_e} M dK = \frac{\sigma_o^2 t}{6E} \tag{27}$$

Since in the peeling test of thin copper film, the curvature K_B is large compared to K_e, one needs to evaluate the contribution to Ψ along (AB). The relationship between the moment M and the curvature K is given in that case by Eq. (10). With the definition $F(-\frac{2\gamma K}{\sqrt{3}}, \frac{t}{2}) = -\exp(-\frac{\gamma K t}{\sqrt{3}}) \left(\frac{t\sqrt{3}}{4\gamma K} + \frac{3}{4\gamma^2 K^2} \right)$, and with a change of variable $u = \frac{\gamma K t}{\sqrt{3}}$, one easily gets :

$$\int_{K_e}^{K_B} F(-\frac{2\gamma K}{\sqrt{3}}, \frac{t}{2}) dK = \frac{3}{4\gamma^2} \left[G\left(-\frac{\gamma t}{\sqrt{3}}, K_B \right) - G\left(-\frac{\gamma t}{\sqrt{3}}, K_e \right) \right] \tag{28}$$

where $G(x, y) = \frac{\exp(xy)}{y}$. The contribution linked to the term $F(-\frac{2\gamma K}{\sqrt{3}}, h)$ with $h = \frac{\sigma_o \sqrt{3}}{2EK}$ is evaluated in a straightforward manner, so the plastic dissipation along the path (AB) is :

$$\begin{aligned} \int_{K_e}^{K_B} = {} & \frac{\alpha t^2}{2\sqrt{3}} (K_B - K_e) + (\frac{\sigma_o}{\sqrt{3}} - \frac{\sqrt{3}\alpha}{2}) \frac{\sigma_o^2}{E^2} (\frac{1}{K_e} - \frac{1}{K_B}) \\ & - \frac{\sqrt{3}\beta}{\gamma^2} \left[G\left(-\frac{\gamma t}{\sqrt{3}}, K_B \right) - G\left(-\frac{\gamma t}{\sqrt{3}}, K_e \right) \right] \\ & + \frac{\sqrt{3}\beta}{\gamma} \exp(-\frac{\gamma \sigma_o}{E}) (\frac{\sigma_o}{E} + \frac{1}{\gamma}) (\frac{1}{K_B} - \frac{1}{K_e}) \end{aligned} \tag{29}$$

For the unloading path (BC), the contribution to Ψ is readily :

$$\int_{K_B}^{K_B - K_B^*} M dK = -M_B K_B^* + \frac{E t^3}{18} (K_B^*)^2 \tag{30}$$

The last term corresponding to the reverse plastic loading phase (CD) is the most complex contribution and can not be estimated in closed form expression in the general case. Indeed, the expression of M is given by Eq. (15) where an integral term is already present. In addition, it is related to the position of the elastic-plastic transition h' defined by an implicit relation (13). Therefore one

can simply noticed that :

$$\int_{K_B-K_B^*}^{0} MdK = \left[\frac{8EK_Bh_B^3}{9} - \frac{2\alpha}{\sqrt{3}}(h_B^2 + \frac{t^2}{4}) + \frac{4\beta}{\sqrt{3}}F(-\frac{2\gamma K_B}{\sqrt{3}}, h_B)\right](K_B^* - K_B) + I \tag{31}$$

where the term I is provided in Eq. (21). As mentioned in Section 2, for metallic film when K_B and γ have large values, the accumulated strain (14) (resp. $h^{'}$) can be approximated as proposed in Eq. (16) (resp. by $h^{'} = \frac{\sqrt{3}\alpha}{E(K_B-K)}$). After some classical mathematical development, the integral term I is evaluated and the approximate closed form expression (22) is found.

References

ABAQUS (2013) Abaqus v6.13 User's Manual, version 6.13 edn. ABAQUS Inc., Richmond, USA

Aravas N, Kim K, Loukis M (1989) On the mechanics of adhesion testing of flexible films. Materials Science and Engineering, A 107:159–168

Girard G, Jrad M, Bahi S, Martiny M, Mercier S, Bodin L, Nevo D, Dareys S (2018) Experimental and numerical characterization of thin woven composites used in printed circuit boards for high frequency applications. Composite structures 193:140 – 153

Hill R (1950) The mathematical theory of plasticity. Oxford University Press, Oxford

IPC (1994) Peel strength of metallic clad laminates, IPC-TM-650 2.4.8, Institute for Interconnecting and Packaging Electronic Circuits, www.ipc.org/TM/2.4.8c.pdf

Kendall K (1973) Shrinkage and peel strength of adhesive joints. Journal of Physics D: Applied Physics 6(15):1782–1787

Kendall K (1975) Thin-film peeling-the elastic term. Journal of Physics D: Applied Physics 8(13):1449–1452

Kim J, Kim K, Kim Y (1989) Mechanical effects in peel adhesion test. J Adhesion Sci Technol 3:175–187

Kim K, Aravas N (1988) Elastoplastic analysis of the peel test. International Journal of Solids and Structures 24:417–435

Kim K, Kim J (1988) Elasto-plastic analysis of the peel test for thin film adhesion. Transactions of the ASME 110:266–273

Kinloch A, Lau C, JG W (1994) The peeling of flexible laminates. International Journal of Fracture 66:45–70

Martiny P, Lani F, Kinloch A, Pardoen T (2008) Numerical analysis of the energy contributions in peel tests : a steady-state multilevel finite element approach. International Journal of Adhesion and Adhesives 28:222–236

Moidu K, Sinclair A, Spelt J (1998) On the determination of fracture energy using the peel test. Journal of Testing and Evaluation 26:247–254

Molinari A, Ravichandran G (2008) Peeling of elastic tapes: Effects of large deformations, pre-straining, and of a peel-zone model. The Journal of Adhesion 84(12):961–995

Ortiz M., Pandolfi A. (1999) Finite-deformation irreversible cohesive elements for three-dimensional crack-propagation analysis. International journal for numerical methods in engineering 44:1267–1282

Rivlin R (1944) The effective work of adhesion. Paint Technology 9:215–218

Song J, Yu J (2002) Analysis of T-peel strength in a Cu/Cr/Polyimide system. Acta Materialia 50:3985–3994

Thouless MD, Yang QD (2008) A parametric study of the peel test. International Journal of Adhesion and Adhesives 28:176–184

Tvergaard V, Hutchinson J (1993) The influence of plasticity on mixed mode interface toughness. Journal of the Mechanics and Physics of Solids 41:1119–1135

Voce E (1948) The relationship between stress and strain for homogeneous deformations. J Inst Metals 74:537–562

Wei Y (2004) Modeling non linear peeling of ductile thin films - critical assessment of analytical bending models using FE simulations. International Journal of Solids and Structures 41:5087–5104

Wei Y, Hutchinson J (1998) Interface strength, work of adhesion and plasticity in peel test. International Journal of Fracture 93:315–333

Wei Y, Zhao H (2008) Peeling experiments of ductile thin films along ceramic substrates - critical assessment of analytical models. International Journal of Solids and Structures 45:3779–3792

Williams J, Kauzlarich J (2005) The influence of peel angle on the mechanics of peeling flexible adherends with arbitrary load - extension characteristics. Tribology International 38:951–958

Yang QD,Thouless MD, Ward SW (2000) Analysis of the symmetrical 90^o- peel test with extensive plastic deformation. Journal of Adhesion 72:115–132

Yang QD,Thouless MD (2001) Mixed-mode fracture analyses of plastically-deforming adhesive joints. International Journal of Fracture 110:175–187

Zhao H, Wei Y (2007) Determination of interface properties between micron-thick metal film and ceramic substrate using peel test. International Journal of Fracture 144:103–112